Supplementary Information (ESI)

Adsorption properties of M-UiO-66 (M = Zr (IV); Hf (IV) or Ce (IV)) with BDC or PDC linker

Diego González[a], Cesar Pazo-Carballo[a,b,d*], Esteban Camú [c,d], Yoan Hidalgo-Rosa [d,e], Ximena Zarate[d,e], Néstor Escalona[b,c,d,], Eduardo Schott[a,d*]

[a] *Departamento de Química Inorgánica, Facultad de Química y Farmacia, Centro de Energía UC, Pontificia Universidad Católica de Chile, Avenida Vicuña Mackenna 4860, Santiago, Chile*
[b] *Departamento de Química Física, Facultad de Química y Farmacia, Pontificia Universidad Católica de Chile, Avenida Vicuña Mackenna 4860, Santiago, Chile Santiago, Chile*
[c] *Departamento de Ingeniería Química y Bioprocesos, Escuela de Ingeniería, Pontificia Universidad Católica de Chile, Avenida Vicuña Mackenna 4860, Macul, Santiago, Chile.*
[d] *Millennium Nuclei on Catalytic Processes towards Sustainable Chemistry (CSC)-Chile.*
[e] *Instituto de Ciencias Químicas Aplicadas, Theoretical and Computational Chemistry Center, Facultad de Ingeniería, Universidad Autónoma de Chile, Av. Pedro de Valdivia 425, Santiago, Chile.*

*edschott@uc.cl

Contents

Chemicals

Ammonium cerium (IV) nitrate (98%, $(NH_4)_2Ce(NO_3)_6$), 1,4-benzenedicarboxylic acid (98%, H_2BDC), 2,5-pyridinedicarboxylic acid (98%, H_2PDC), Zirconium(IV) chloride (99%, $ZrCl_4$), Zirconyl (VI) Chloride octahydrate (98%, $ZrOCl_2{\cdot}8H_2O$), (Hafnium (IV) chloride (99%, $HfCl_4$), n-butylamine ($CH_3(CH_2)_3NH_2$, ≥99%), formic acid (96%, CH_2O_2), and Sodium nitrate ($NaNO_3$, ACS reagent, ≥99.0 %) were purchased from Sigma-Aldrich. Acetic acid (CH_3COOH, 98.5-100.5%), Acetone (C_3H_6O, 99%), hydrochloric acid (HCl, 98%), Sodium hydroxide (NaOH, 99%), N,N'-dimethylformamide (DMF, 99 wt.%), Ethanol (C_2H_60, 99.9%), Methanol (CH_3OH, 99.9%) was supplied by Fine Chemical Co. Ltd. and reagent alcohols were purchased from Macron Chemicals. Carbon dioxide (CO_2, 99.999%).

Synthesis Procedures

Synthesis of Zr (IV) and Hf (IV) UiO-66[1]

0,5 mmol of $ZrCl_4$ (or $HfCl_4$) was added on a 20 mL vial with 5 mL of DMF and 1 mL of concentrated HCl. After sonication for 10 minutes (for dissolving), 10 mL of DMF was added with 0,6 mmol of Terephthalic acid (H_2BDC) and 10 additional minutes of sonication before being heated ay 80˚C for 12 hours. The resulting solid was separated and washed by centrifugation at 8000 rpm for 10 minutes with DMF (2x10 mL) and then with ethanol (2x10 mL). The MOF was dried under reduced pressure at room temperature for 3 days.

Synthesis of Ce-UiO-66[2]

On a 20 mL vial, the following reactive were added: first 1,5 mmol of terephthalic acid with 7,5 mL of DMF and then 2,4 mL of $(NH_4)_2[Ce(NO_3)_6]$ 0,533 M. The vial was heated using an aluminum heater block under stirring for 30 minutes at 100˚C. The resulting light-yellow solid was separated and washed by centrifugation at 8000 rpm for 10 minutes (sometimes 20) with DMF (3x10 mL) and then with ethanol (3x10 mL). The MOF was dried under reduced pressure at room temperature for 3 days.

Synthesis of Zr-UiO-66-PDC[3]

4,4 mmol of 2,5-pirydinedicarboxilic acid (H_2PDC) and 4,4 mmol of $ZrOCl_2 \cdot 8\ H_2O$ were mixed in 45 mL formic acid and 5 mL water in a round bottom flask. The mixture was heated at 120˚C under reflux for 3 hours. The reaction was quenched by placing the round bottom flask under cold water. The resulting solid was separated and washed by centrifugation at 8000 rpm for 10 minutes with water (2x10 mL) and ethanol (2x10 mL). The MOF was dried under reduced pressure at room temperature for 3 days.

Synthesis of Hf-UiO-66-PDC[3]

5 mmol of H_2PDC and 5 mmol of $HfCl_4$ were mixed in 25 mL of acetic acid and 25 mL of water in a round bottom flask. The mixture was heated at 120˚C under reflux for 3 hours. The reaction was quenched by placing the round bottom flask under cold water. The resulting solid was separated and washed by centrifugation at 8000 rpm for 10 minutes with water (2x10 mL) and then with ethanol (2x10 mL). The MOF was dried under reduced pressure at room temperature for 5 days.

Synthesis of Ce-UiO-66-PDC[3]

10 mmol of H_2PDC and 10 mmol of $(NH_4)_2[Ce(NO_3)_6]$ were mixed in 5 mL of concentrated HNO_3 and 45 mL of water in a round bottom flask. The mixture was heated at 90˚C under reflux for 30 minutes. The reaction was quenched by placing the round bottom flask under cold water. The resulting solid was separated and washed by centrifugation at 8000 rpm for 10 minutes (sometimes 20) with water (2x10 mL) and then with ethanol (2x10 mL). The MOF was dried under reduced pressure at room temperature for 3 days.

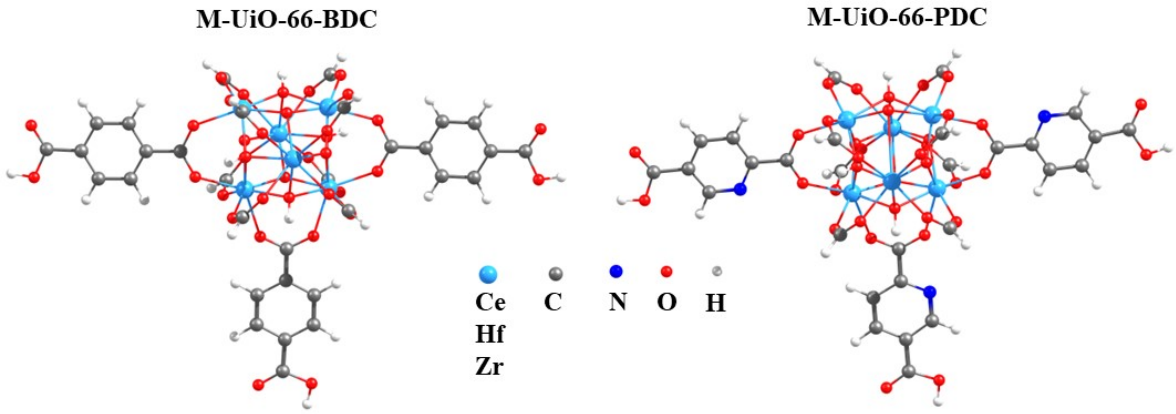

Figure S1. Structural Model $M_6O_4(OH)_4(Linker)_3(HCOO^-)_8]$ (M = Zr (IV), Ce (IV), and Hf (IV); linker = BDC or PDC), representation of the M-UiO-66 truncated.

Characterization data

FT-IR spectra

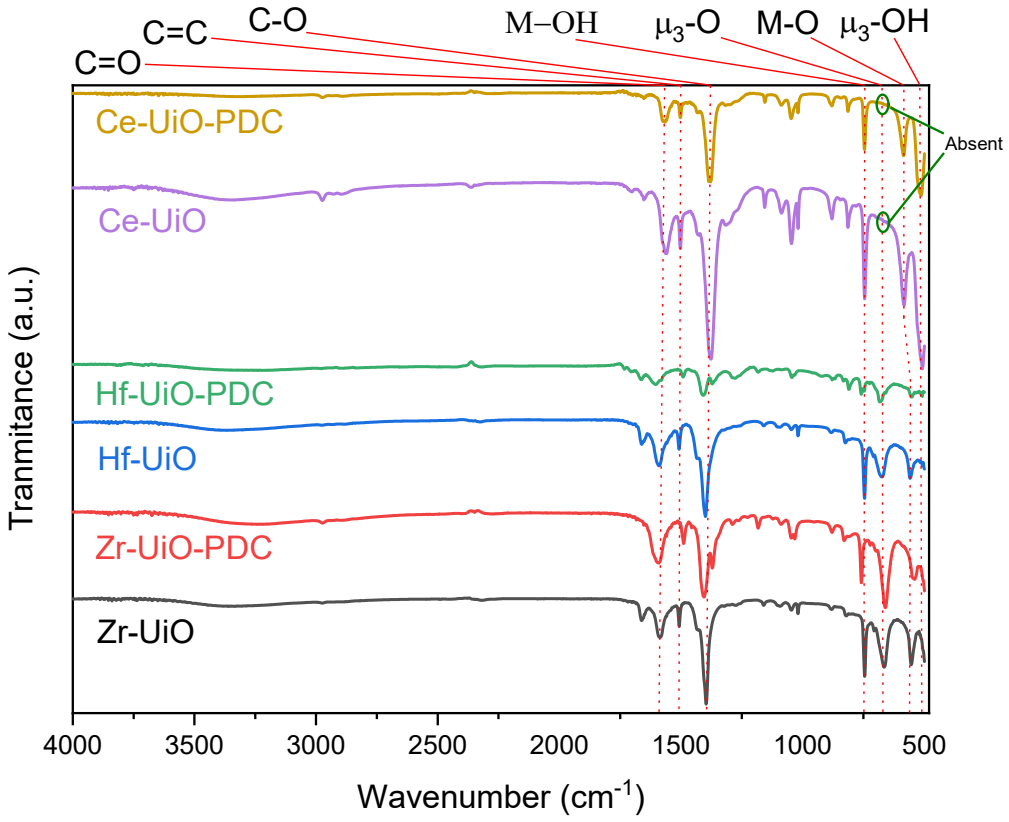

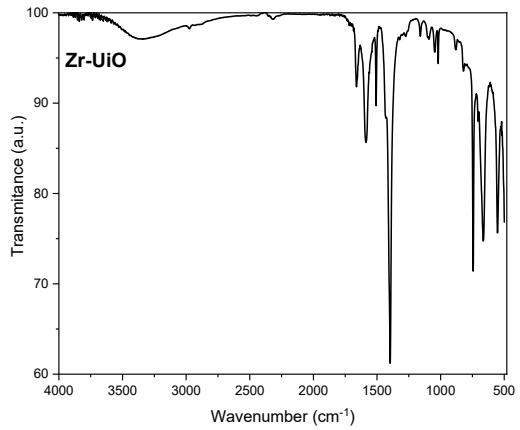

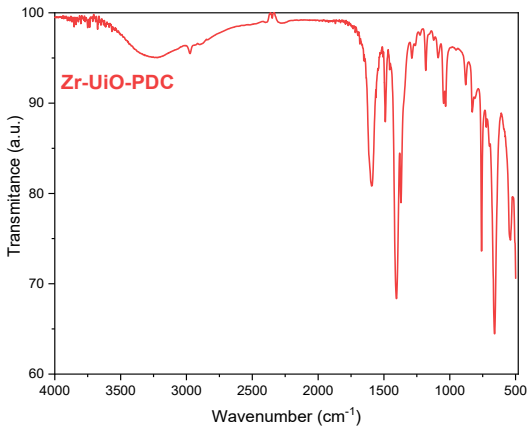

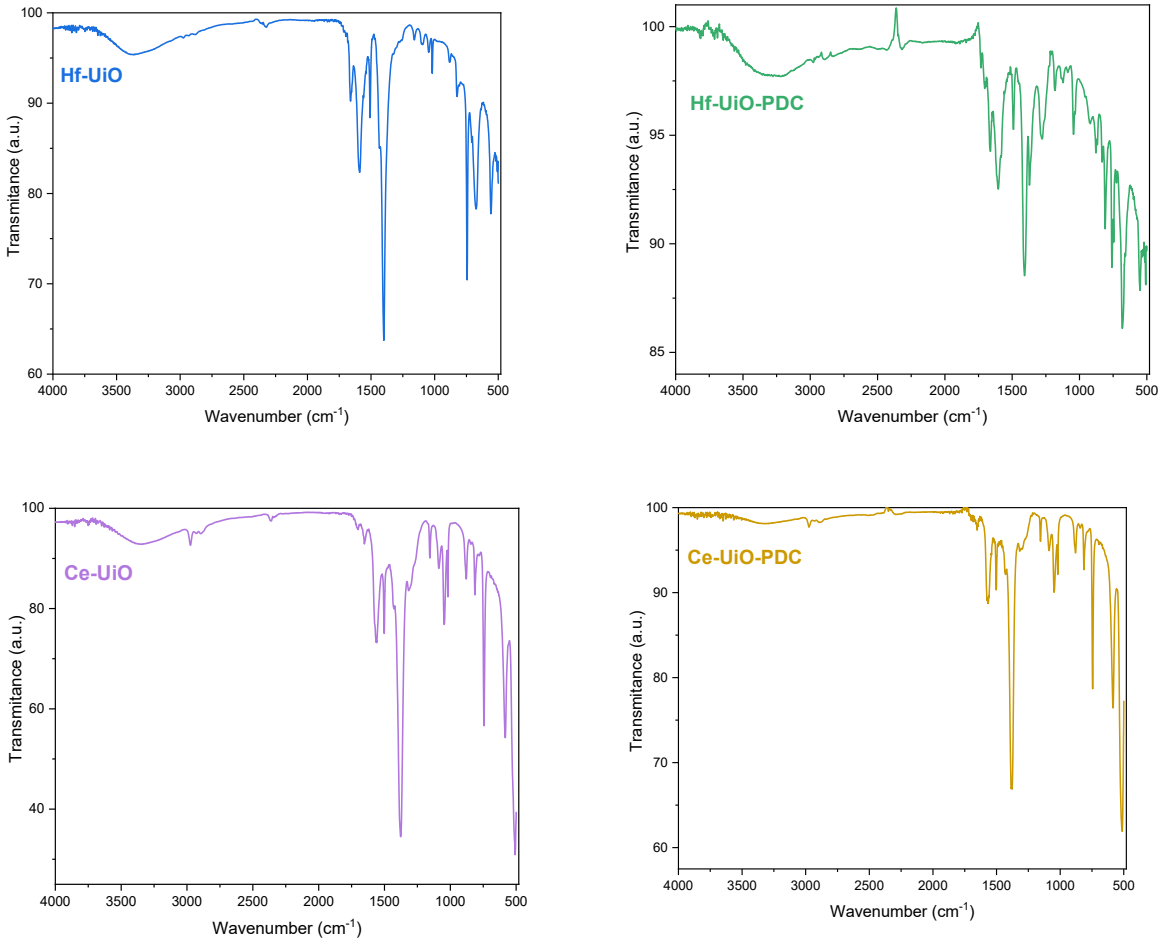

Figure S2. FT-IR spectra of M-UiO-66 (M = Zr (IV), Ce (IV), Hf (IV)) with BDC or PDC linker.

Powder x-ray diffraction

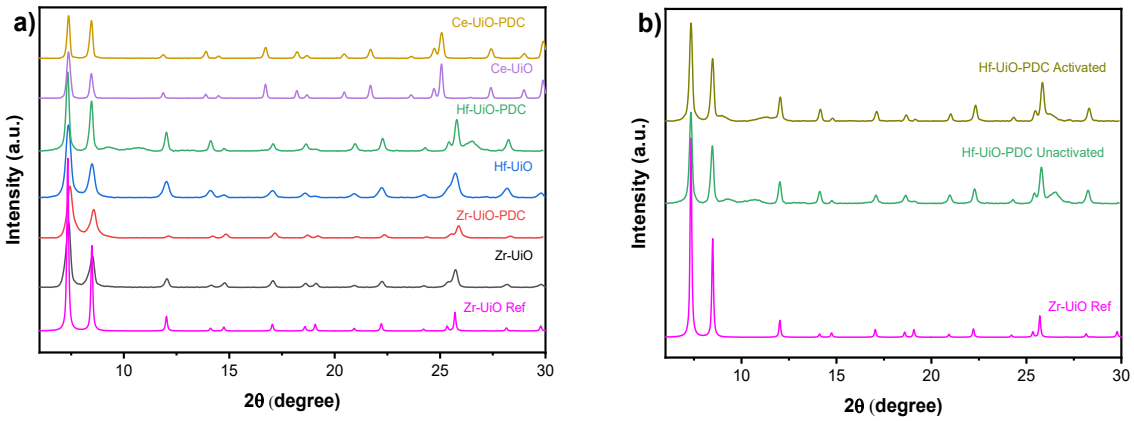

Figure S3. (a) PXRD pattern of M-UiO-66 (M = Zr (IV), Ce (IV), Hf (IV)) with BDC or PDC linker and (b) PXRD of Hf-UiO-66-PDC before and after activation process at 180˚C under vacuum for 4 hours.

Table S1. Crystallite size and crystallinity percentage of M-UiO-66 (M = Zr (IV), Ce (IV), Hf (IV)) with BDC or PDC linker.

Materials	**Crystallite size (nm)**	**Crystallinity (%)**
Zr-UiO-66	25.5	99.6
Zr-UiO-66-PDC	44.8	98.3
Ce-UiO-66	40.5	97.0
Ce-UiO-66-PDC	52.2	95.6
Hf-UiO-66	31.6	98.3
Hf-UiO-66-PDC	52.7	80.3

N_2 adsorption-desorption analysis

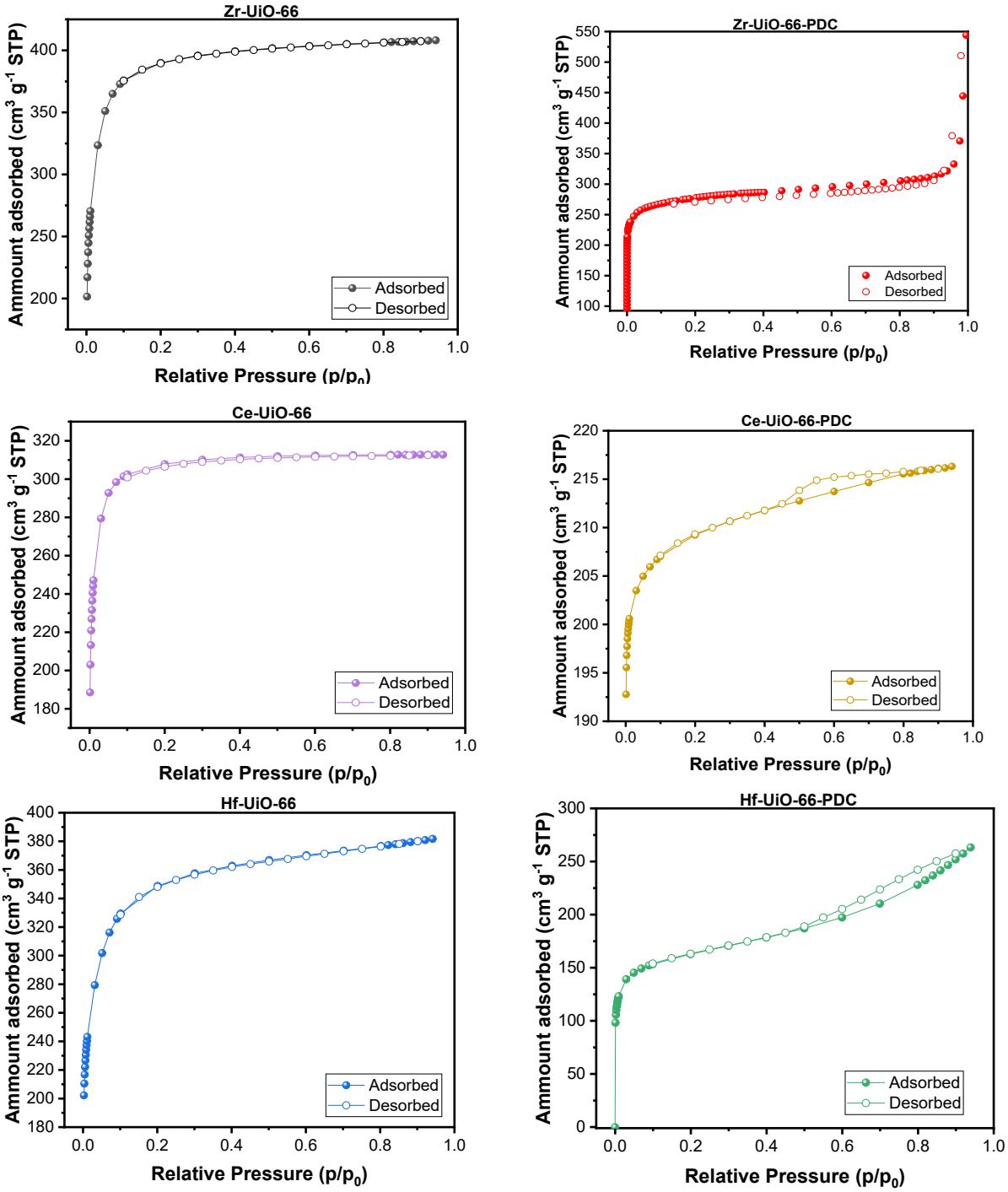

Figure S4. Nitrogen isotherm at 77 K of M-UiO-66 (M = Zr (IV), Ce (IV), Hf (IV)) with BDC or PDC linker.

Table S2. Textural properties of MOFs.

Compound	$S_{BET}\ [m^2g^{-1}]$	$V_{Micro}\ [cm^3g^{-1}]$	$V_{total}\ [cm^3g^{-1}]$	Bibliographic $S_{BET}\ [m^2g^{-1}]$	V_{Meso} [cm^3 g^{-1}]
Zr-UiO-66	1188	0.46	0.63	1105[4]	0.17
Zr-UiO-66-PDC	1083	0.42	0.51	1376[3]	0.09
Ce-UiO-66	925	0.42	0.48	1282[2]	0.06
Ce-UiO-66-PDC	626	0.30	0.33	768[3]	0.03
Hf-UiO-66	1196	0.42	0.59	358-749[5]	0.17
Hf-UiO-66-PDC	509	0.16	0.41	383[3]	0.25

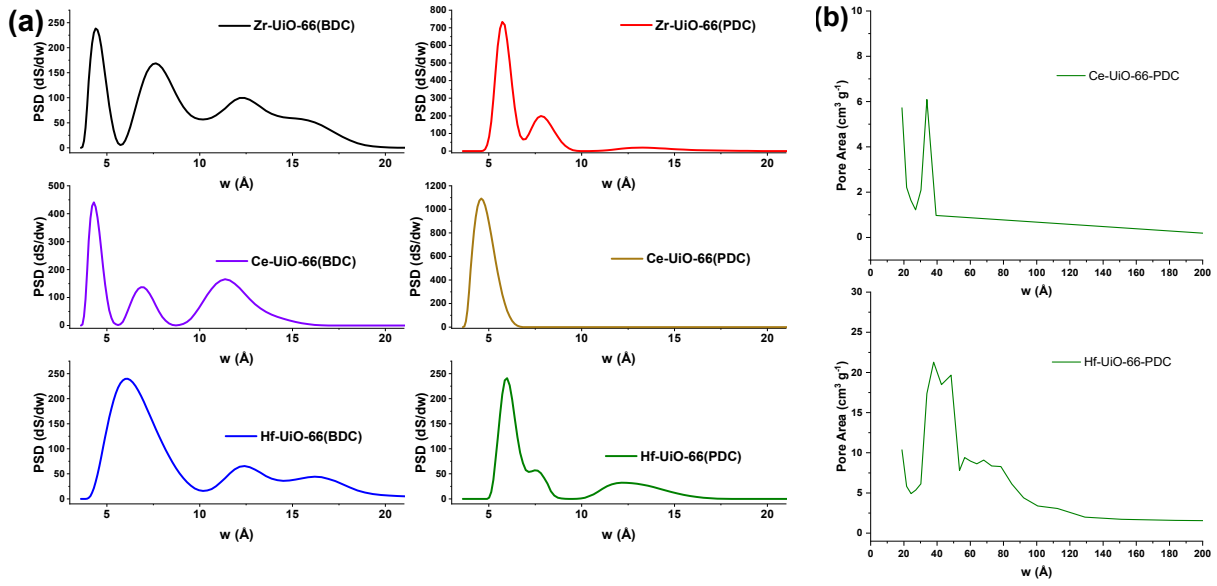

Figure S5. (a) Pore size distribution of MOFs calculated by NLDFT and (b) mesoporous region for Hf and Ce UiO-66-PDC calculated by Barrett-Joyner-Halenda (BJH) method.

Defect chemistry

Determination of defect concentration varies between BDC and PDC MOFs due to the hydrophobicity of M-UiO-66-PDC materials who impeded the correct measurement of *Glass* pH Electrode during potentiometric titration.

Defect determination for M-UiO-66 via titration

Defect determination via potentiometric titration was calculated according to Klet et al.[6]

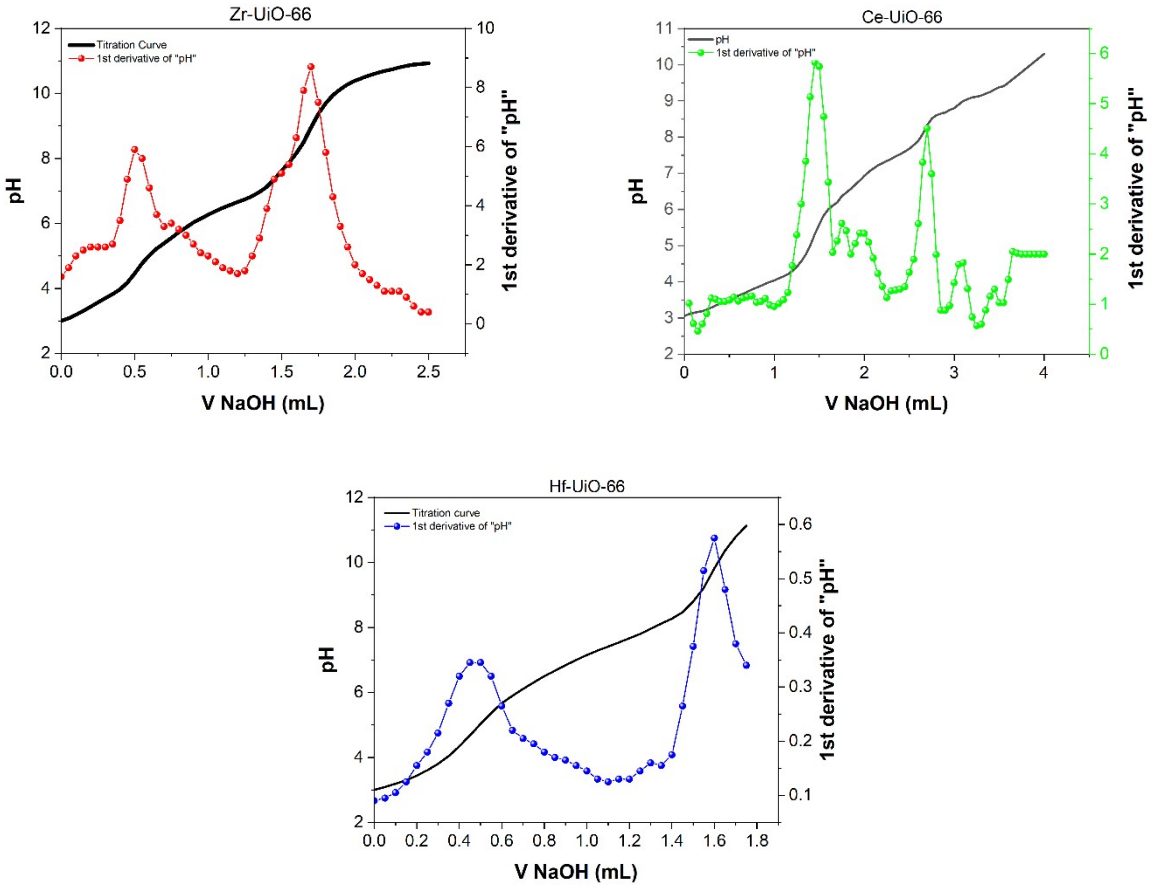

Figure S6. Potentiometric titrations of M-UiO-66 for defect determination.

Table S3 Defect determination for M-UiO-66

Material	Missing Linker	Molecular Formula	**MW (g mol^{-1})**
Zr-UiO-66	0,85	$Zr_6O_4(OH)_4(C_8H_4O_4)_{5.15}[(H_2O)(OH)]_{1.7}$	1583,82
Ce-UiO-66	1,85	$Ce_6O_4(OH)_4(C_8H_4O_4)_{4.15}[(H_2O)(OH)]_{3.7}$	1783,1
Hf-UiO-66	1,05	$Hf_6O_4(OH)_4(C_8H_4O_4)_{4.95}[(H_2O)(OH)]_{2.1}$	2085,4

Defect determination for M-UiO-66-PDC via TGA

Defect determination via TGA was calculated according to Lázaro.[7]

Table S4 Defect determination for M-UiO-66-PDC

Material	Wexp.Pla	NLexp	Missing Linker	Molecular Formula
Zr-UiO-66-PDC	186	4,1	1,9	$Zr_6O_4(OH)_4(C_7NH_4O_4)_{4.1}[(H_2O)(OH)]_{3.8}$
Ce-UiO-66-PDC	170	4,7	1,3	$Ce_6O_4(OH)_4(C_7NH_4O_4)_{4.7}[(H_2O)(OH)]_{2.6}$
Hf-UiO-66-PDC	167	5,5	0,5	$Hf_6O_4(OH)_4(C_7NH_4O_4)_{5.5}[(H_2O)(OH)]_{1.0}$

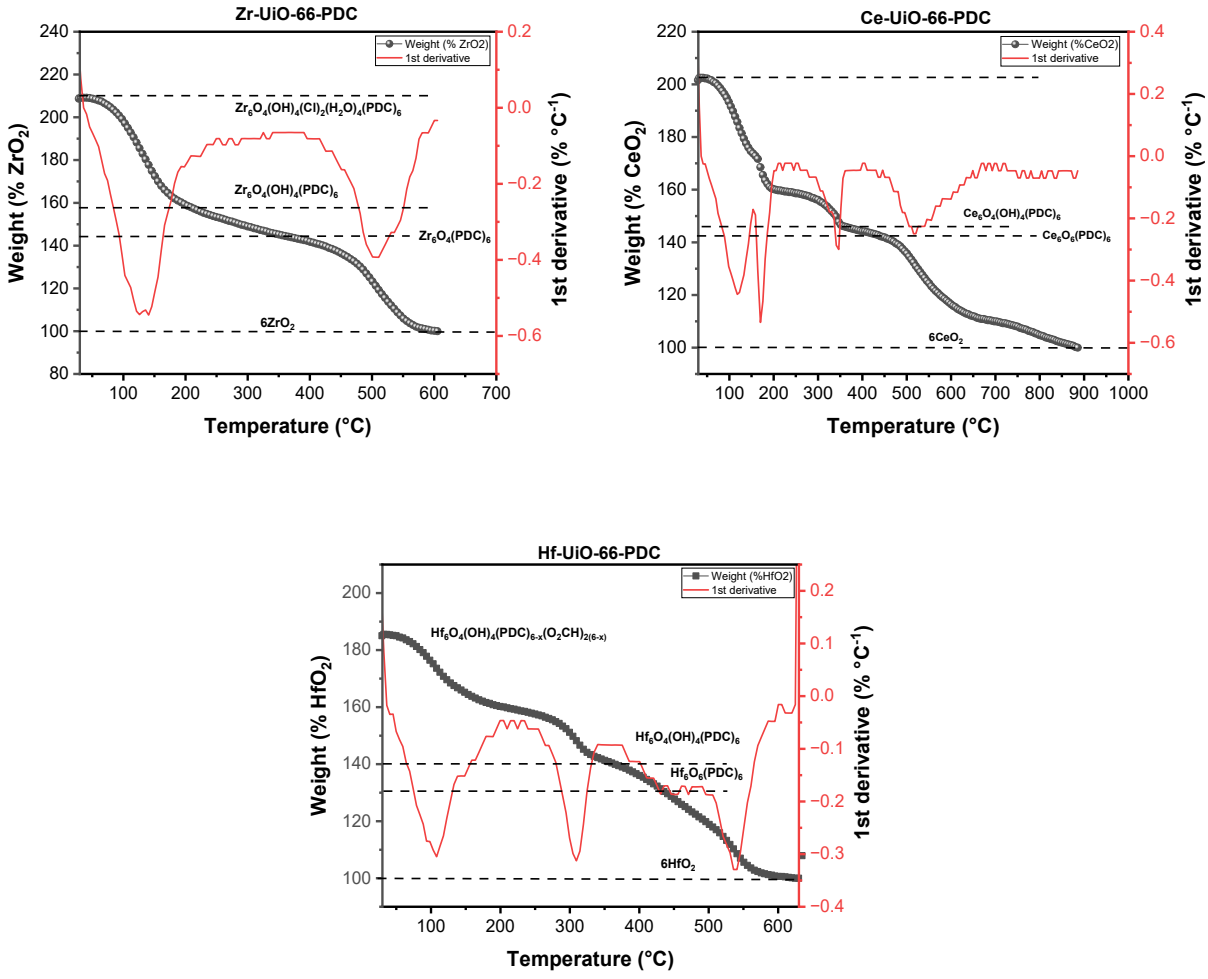

Figure S7. Thermogravimetric analysis of M-UiO-66-PDC for defect determination.

CO_2 adsorption parameters and error range

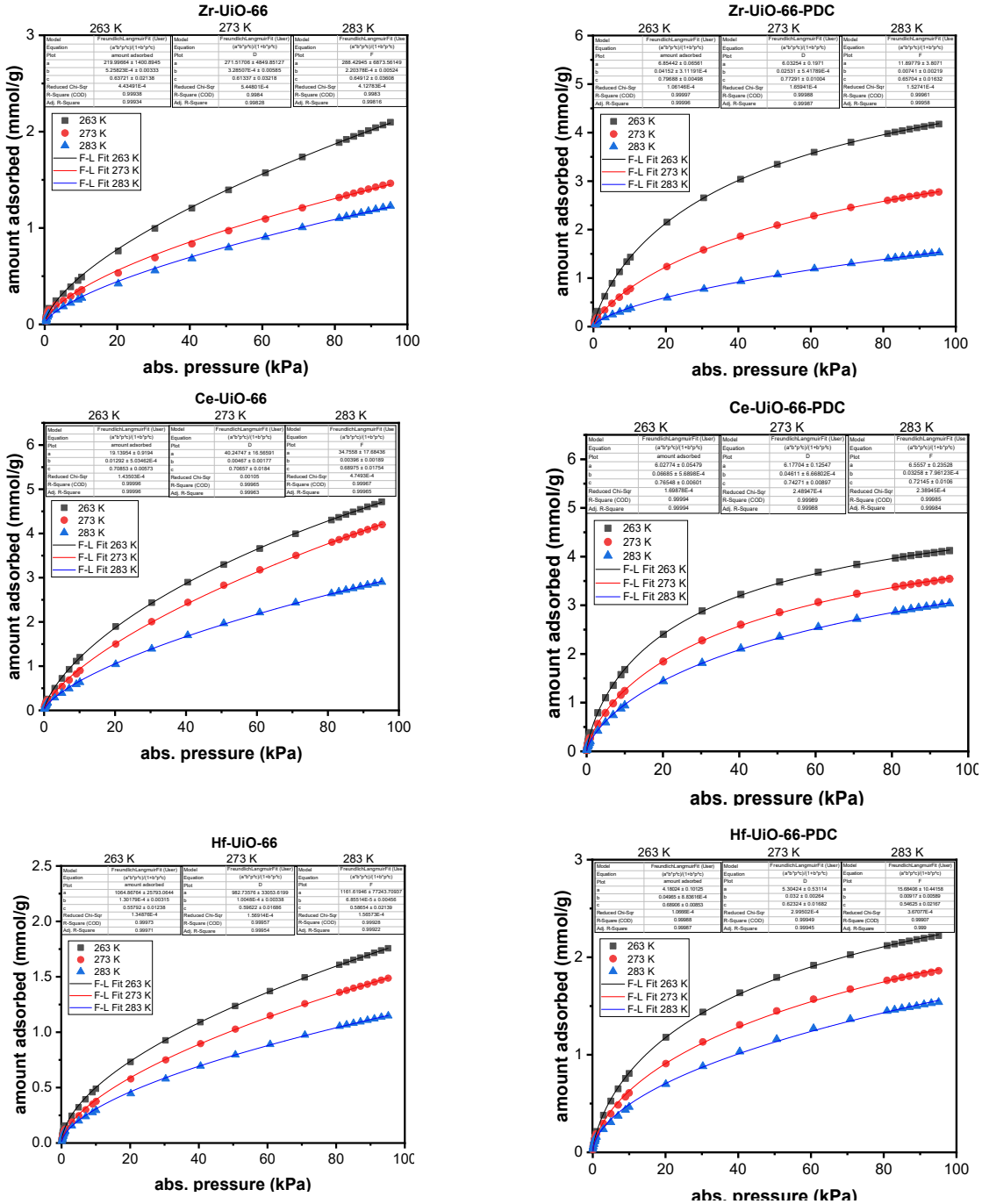

Figure S8. Freundlich-Langmuir fit parameters for each curve.

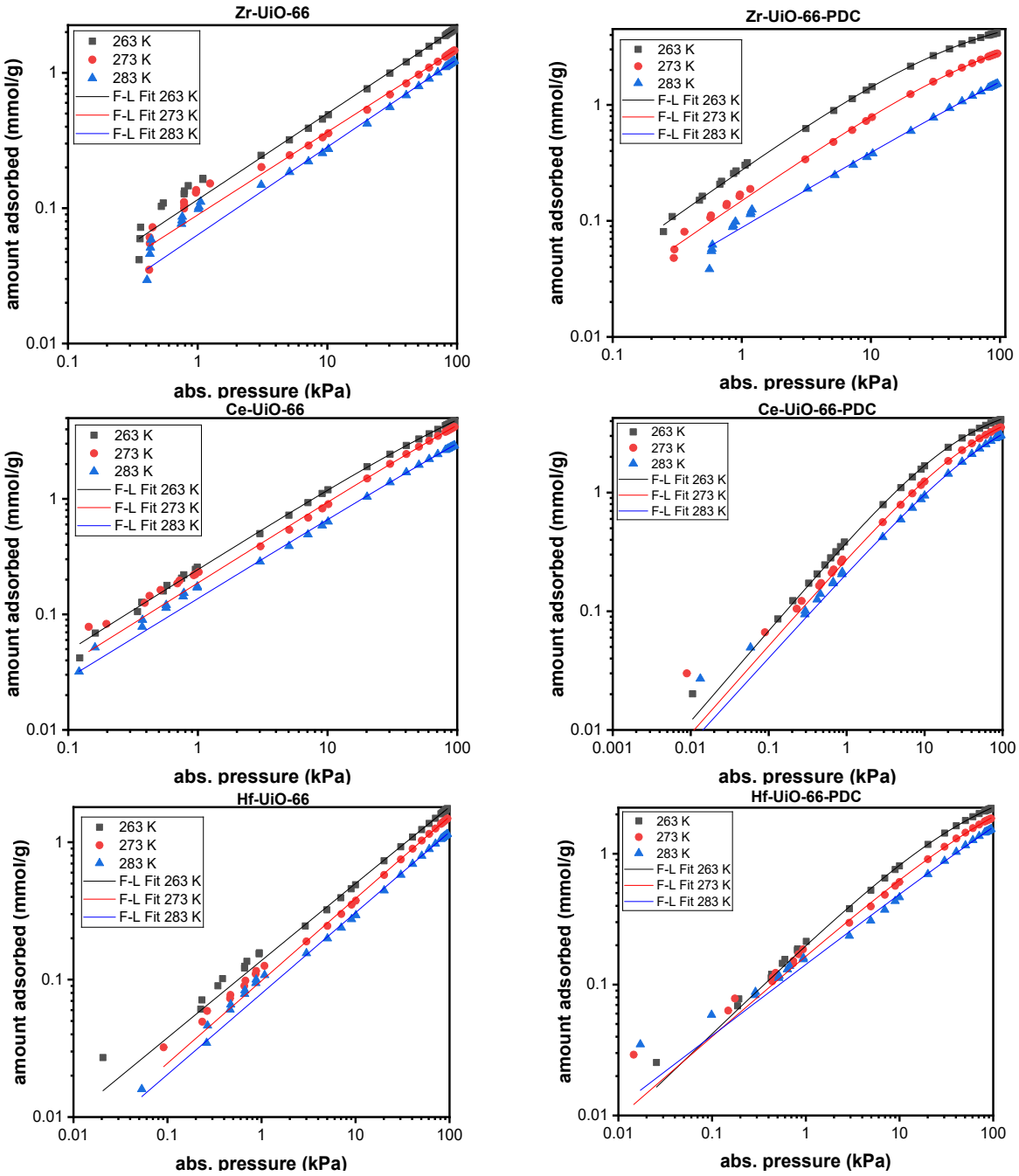

Figure S9. CO_2 adsorption curves under logarithmic scale to visualize the error at low pressures.

Table S5. CO_2 adsorption of the materials at the maximum measured pressure.

Compound	Uptake at 95 kPa and 263 K [mmol g^{-1}]	Uptake at 95 kPa and 273 K [mmol g^{-1}]	Uptake at 95 kPa and 283 K [mmol g^{-1}]
Zr-UiO-66	2.10	1.46	1.23
Zr-UiO-66-PDC	4.18	2.77	1.53
Ce-UiO-66	4.72	4.20	2.90
Ce-UiO-66-PDC	4.12	3.54	3.04
Hf-UiO-66	1.76	1.49	1.15
Hf-UiO-66-PDC	2.22	1.86	1.54

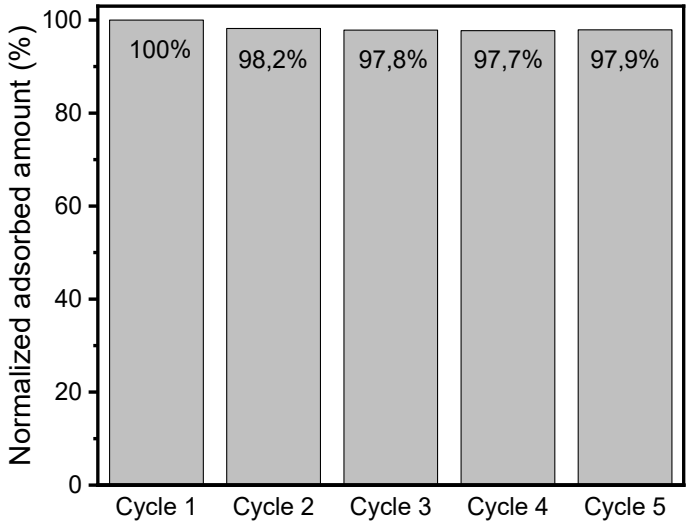

Figure S10. Comparison of adsorption capacity between cycles of Zr-UiO-66-PDC, all cycles have been normalized respective to first cycle.

Computational Analysis

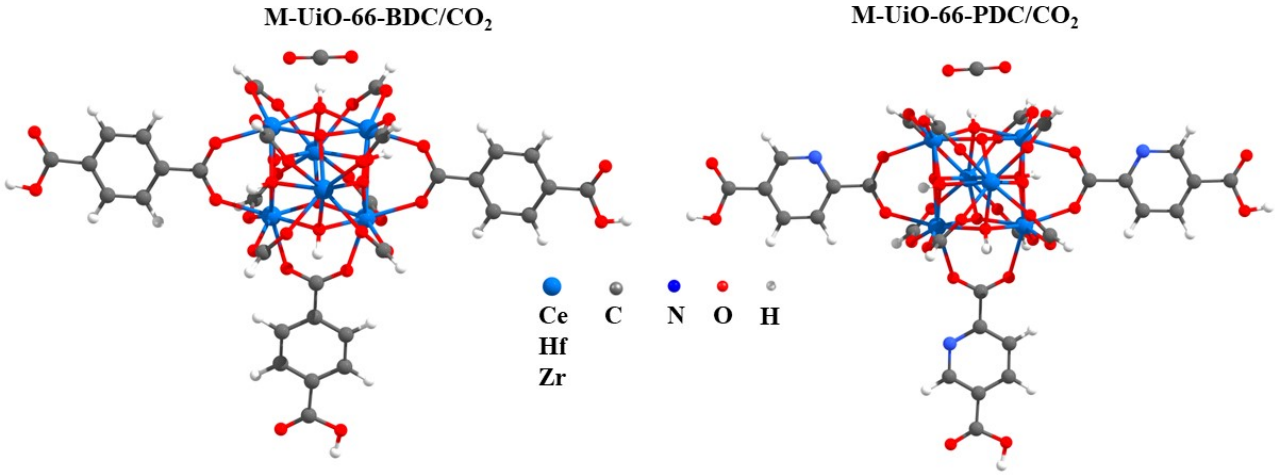

Figure S11. Structural Model $M_6O_4(OH)_4(Linker)_3(HCOO^-)_8]/CO_2$ (M = Zr (IV), Ce (IV), and Hf (IV); linker = BDC or PDC), representation of the M-UiO-66 truncated

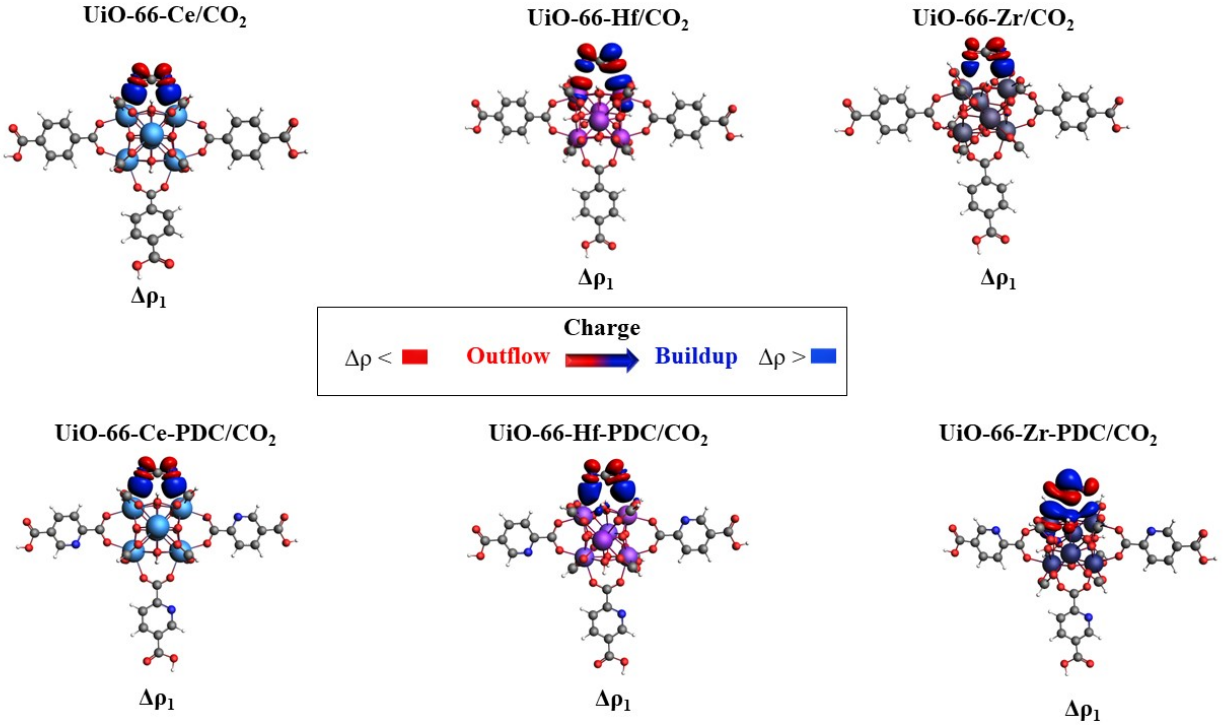

Figure S12. Contours of deformation density channels ($\Delta\rho_1$) with the corresponding energies, in kcal/mol, describing the donor–acceptor interaction in M-UiO-66/CO_2 systems

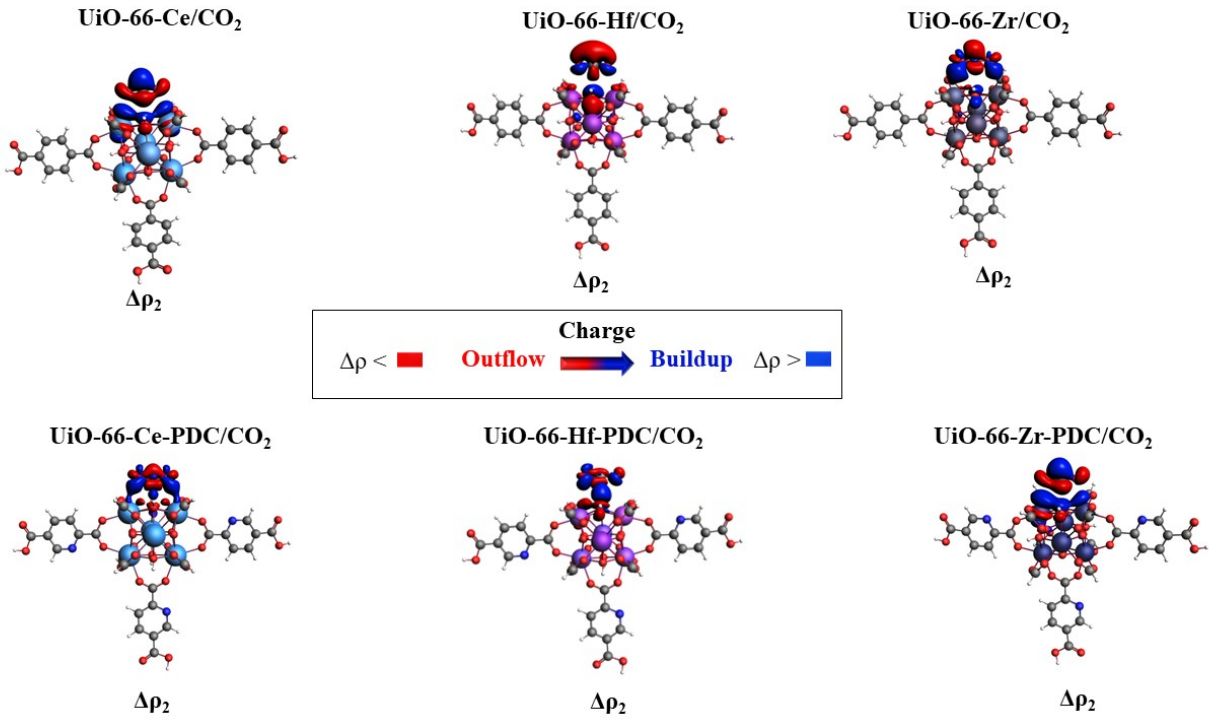

Figure S13. Contours of deformation density channels ($\Delta\rho_2$) with the corresponding energies, in kcal/mol, describing the donor–acceptor interaction in M-UiO-66/CO_2 systems

Table S6. Selected bond lengths and hydrogen bond in the Ground state (S_0) distances (Å) at M06L/ TZ2P/ZORA

Materials/	**M-O1** (M–μ_3-OH)	**M-O2** (M–μ_3-O)	**M-O3** (**M**-OOC-R)
UiO-66-Zr	2.25(5)	2.12(5)	2.21(1)
UiO-66-Ce	2.44(3)	2.28(2)	2.36(0)
UiO-66-Hf	2.26(5)	2.13(4)	2.21(2)
UiO-66-Zr[8]	2.27	2.07	2.23
UiO-66-Ce[9]	2.45	2.25	2.47
UiO-66-Hf[10]	2.27	2.06(7)	2.21
UiO-66-Zr-PDC	2.28(2)	2.24(2)	2.16(4)
UiO-66-Ce-PDC	2.44(8)	2.29(0)	2.36(7)
UiO-66-Hf -PDC	2.27(3)	2.27(4)	2.16(1)

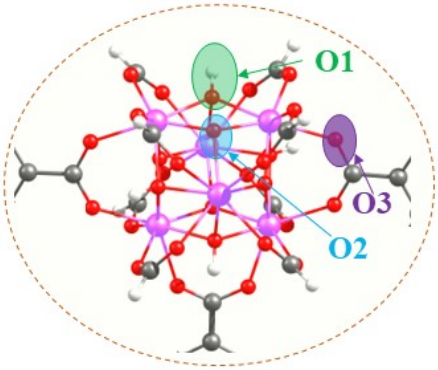

Table S7. Optimized molecular structures of M-UiO-66 at M06L/ TZ2P/ZORA

M-UiO-66/CO_2 System

Ce-UiO-66/CO_2

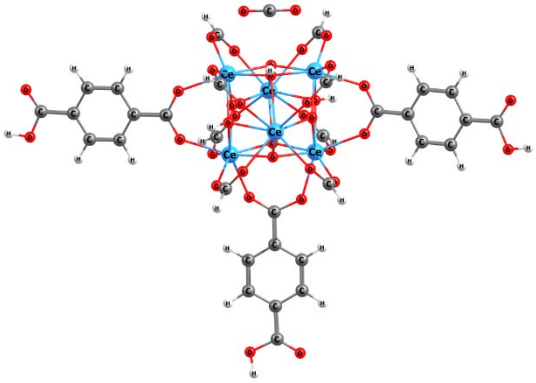

Ce-UiO-66-PDC

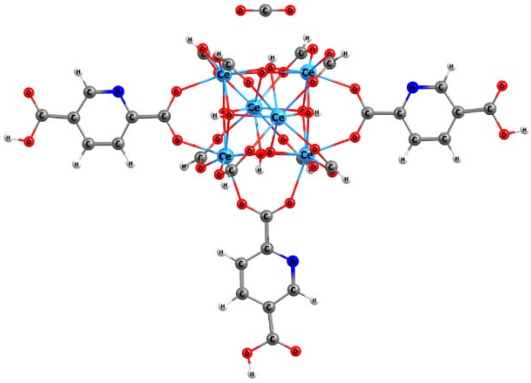

Zr-UiO-66/CO_2

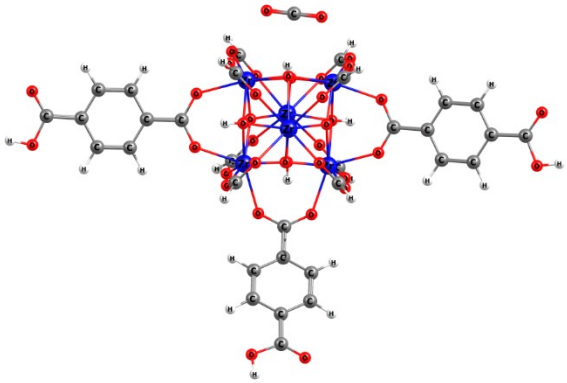

Zr-UiO-66-PDC/CO_2

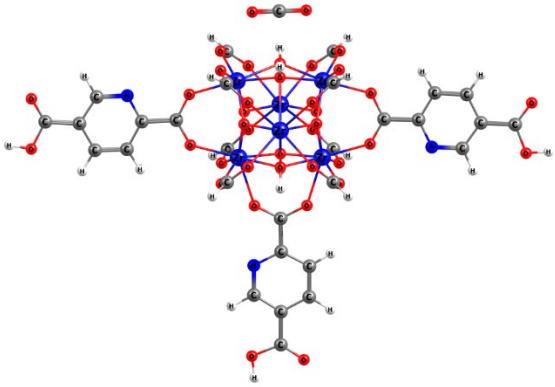

Hf-UiO-66/CO_2

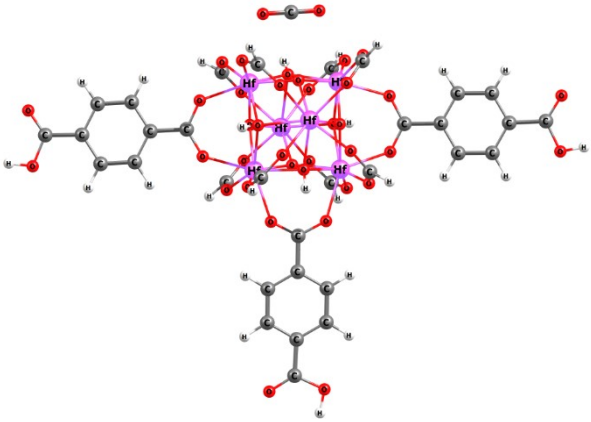

Hf-UiO-66-PDC/CO_2

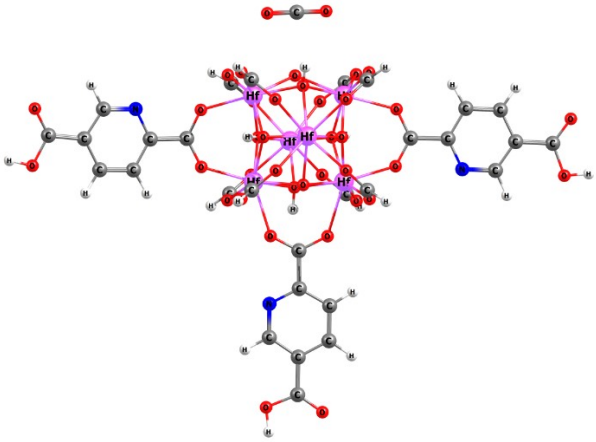

Table S8. Selected bond lengths and hydrogen bond in the Ground state (S_0) distances (Å) at M06-L/ TZ2P/ZORA theoretical level.

Materials/	**M ···CO_2**	**-O-H···CO_2** ($-\mu_3$-OH)	**O ···CO_2** ($-\mu_3$-O)
UiO-66-Ce···CO_2	3.040	3.296	3.362
UiO-66-Zr···CO_2	2.962	3.173	3.231
UiO-66-Hf···CO_2	2.925	3.150	3.180
UiO-66-Ce-PDC···CO_2	3.035	3.300	3.342
UiO-66-Zr-PDC···CO_2	3.181	3.063	3.090
UiO-66-Hf-PDC···CO_2	3.374	3.038	3.025

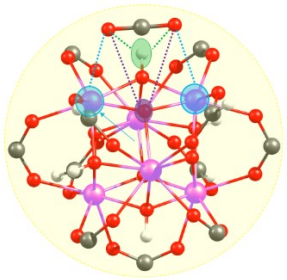

Table S9. Morokuma–Ziegler scheme energy decomposition analysis (EDA), values in kcal/mol, for all interacting systems M-UiO-66/CO_2.

System	**ΔE_{Pauli}**	**ΔE_{Elec}**	**ΔE_{Orb}**	**ΔE_{Disp}**	**ΔE_{Int}**
UiO-66-Zr	16.82	-10.37 (42 %)	-7.54 (31%)	-6.75 (27 %)	**-7.83**
UiO-66-Ce	13.55	-9.28 (42 %)	-6.67 (31%)	-5.91 (27 %)	**-8.31**
UiO-66-Hf	18.82	-12.27 (45 %)	-8.49 (31%)	-6.39 (24 %)	**-8.33**
UiO-66-Zr-PDC	11.75	-8.97 (48 %)	-4.77 (22 %)	-6.02 (29%)	**-8.01**
UiO-66-Ce-PDC	13.67	-9.36 (45%)	-6.85 (24 %)	-5.92 (30 %)	**-8.46**
UiO-66-Hf-PDC	10.54	-8.34 (42 %)	-3.87 (31%)	-5.00 (27 %)	**-6.67**

Kinetics of adsorption

Kinetics data was obtained from the same report of CO_2 adsorption capacity experiments, where the points are collected in a batch system in the relative pressure range of $0.05 \leq P/P_0 \leq 0.99$. That means each point is graphed as an amount adsorbed in function of time. The amount adsorbed is obtained by adding a small known amount of adsorbate (CO_2) and taking the time it takes to the pressure to stop reducing (and that is converted to an adsorbed amount). Then another alicuote of adsorbate is added to graph another point and the process is repeated until de relative pressure reaches the value of 0.99.

Kinetic Model

Table S10. Resume of avrami's kinetic model parameters.

		Avrami fractional-order		
		263 K	273 K	283 K
UiO-66-Zr	K_{Av}	0.03064	0.02994	0.03008
	n_{Av}	3.8283	3.90391	4.30755
	q_e	2.05989	1.4636	1.2108
	R^2	0.99449	0.99075	0.99154
UiO-66-Zr-PDC	K_{Av}	0.02851	0.03326	0.02688
	n_{Av}	3.88066	4.34535	3.57448
	q_e	4.18614	2.72374	1.52613
	R^2	0.99414	0.99597	0.9959
UiO-66-Ce	K_{Av}	0.0309	0.0312	0.03095
	n_{Av}	3.80977	4.50818	4.17657
	q_e	4.62802	4.0901	2.84934
	R^2	0.99717	0.9959	0.99639
UiO-66-Ce-PDC	K_{Av}	0.03156	0.03132	0.03154
	n_{Av}	2.83463	3.52024	3.73543
	q_e	4.15888	3.5137	3.00462
	R^2	0.99681	0.99692	0.99726
UiO-66-Hf	K_{Av}	0.03179	0.03155	0.03154
	n_{Av}	3.7351	3.93656	3.94531
	q_e	1.73921	1.47132	1.13783
	R^2	0.99394	0.99408	0.9922
UiO-66-Hf-PDC	K_{Av}	0.03336	0.03232	0.03301
	n_{Av}	3.69314	4.03082	3.73094
	q_e	2.22111	1.85187	1.54021
	R^2	0.99453	0.99163	0.99177

Table S11. Resume of pseudo-first order and pseudo-second order kinetic model parameters.

		Pseudo-first order				Pseudo-second order		
		263 K	273 K	283 K		263 K	273 K	283 K
UiO-66-Zr	K_1	0.02587	0.01769	0.02224	K_s	0.0024	0.00153	0.00282
	q_e	3.61239	3.38092	2.44738	q_e	6.26893	6.24395	4.40217
	R^2	0.96797	0.95882	0.95719	R^2	0.96625	0.95792	0.9559
UiO-66-Zr-PDC	K_1	0.03099	0.04563	0.02867	K_s	0.00186	0.0052	0.00446
	q_e	6.28184	3.68129	2.36023	q_e	10.35126	5.79622	3.93397
	R^2	0.96464	0.96957	0.98112	R^2	0.96163	0.965	0.97948
UiO-66-Ce	K_1	0.02917	0.02489	0.0235	K_s	0.00136	0.00105	0.00135
	q_e	7.54962	7.57988	5.48316	q_e	12.81406	13.40191	9.76773
	R^2	0.97526	0.95614	0.96598	R^2	0.9733	0.95421	0.96453
UiO-66-Ce-PDC	K_1	0.03865	0.04883	0.04606	K_s	0.00323	0.00535	0.00525
	q_e	5.33483	4.34943	3.89047	q_e	8.20574	6.51222	5.9926
	R^2	0.97512	0.97654	0.97767	R^2	0.9709	0.97177	0.97346
UiO-66-Hf	K_1	0.03381	0.02932	0.02889	K_s	0.00469	0.00408	0.00512
	q_e	2.6633	2.47306	1.93022	q_e	4.42619	4.2417	3.31967
	R^2	0.96735	0.96549	0.961	R^2	0.96476	0.96344	0.95894
UiO-66-Hf-PDC	K_1	0.04893	0.04521	0.04314	K_s	0.00764	0.00754	0.00831
	q_e	2.8672	2.51033	2.12021	q_e	4.402	3.95864	3.37799
	R^2	0.96134	0.95555	0.96258	R^2	0.95611	0.95092	0.95862

For pseudo-first and pseudo-second order the time $t = 0$ was determined at the point where $dq_t/dt \neq 0$.

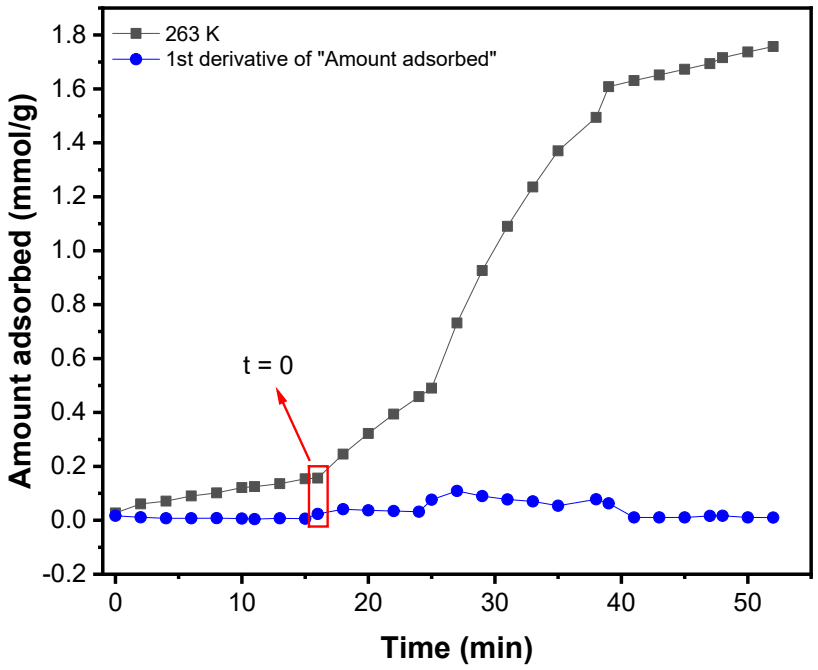

Figure S14. Example of the determination of time $t = 0$ for the non-linear fit of pseudo-first and pseudo-second order kinetic models.

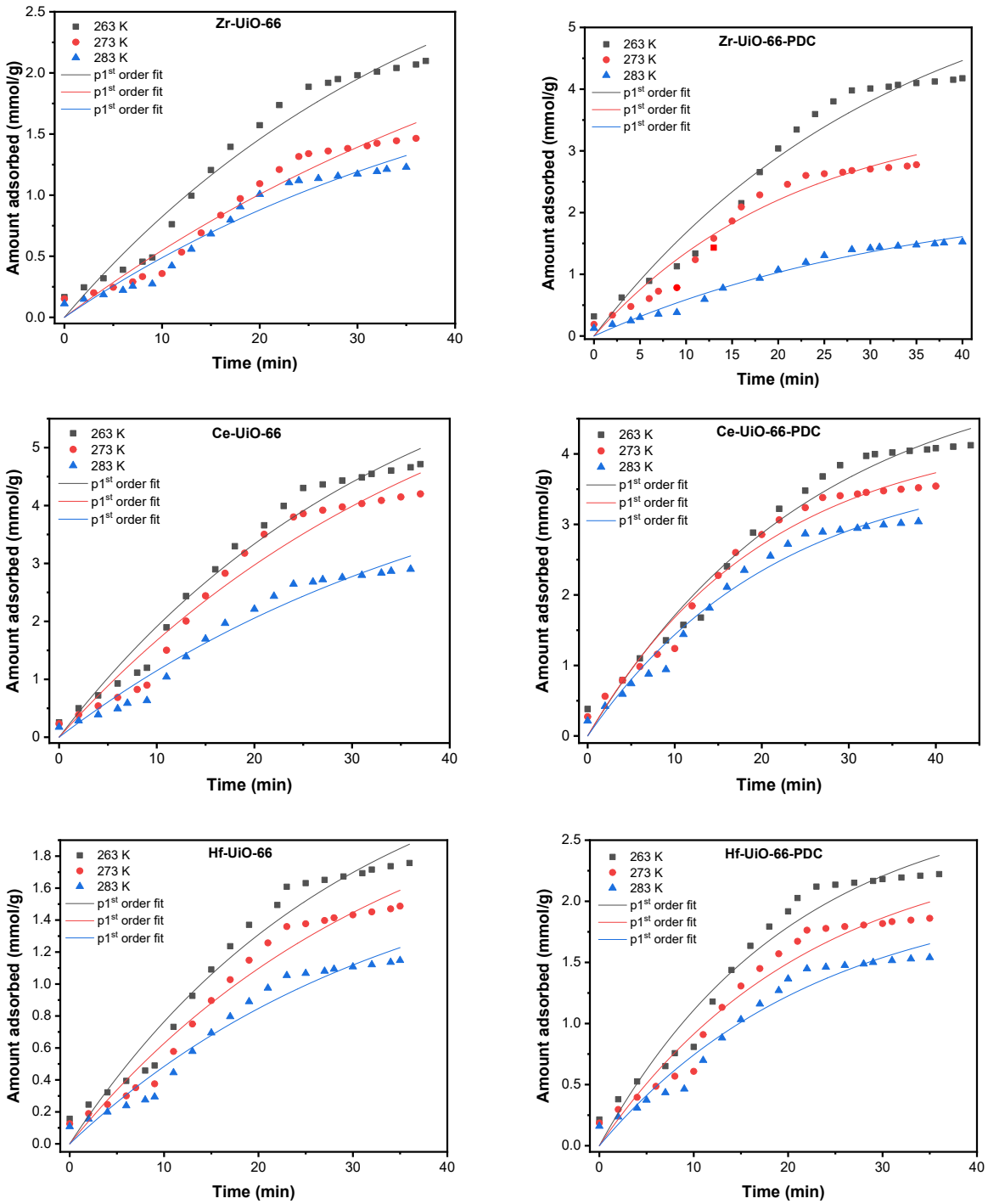

Figure S15. Non-linear fit of pseudo-first order kinetic model.

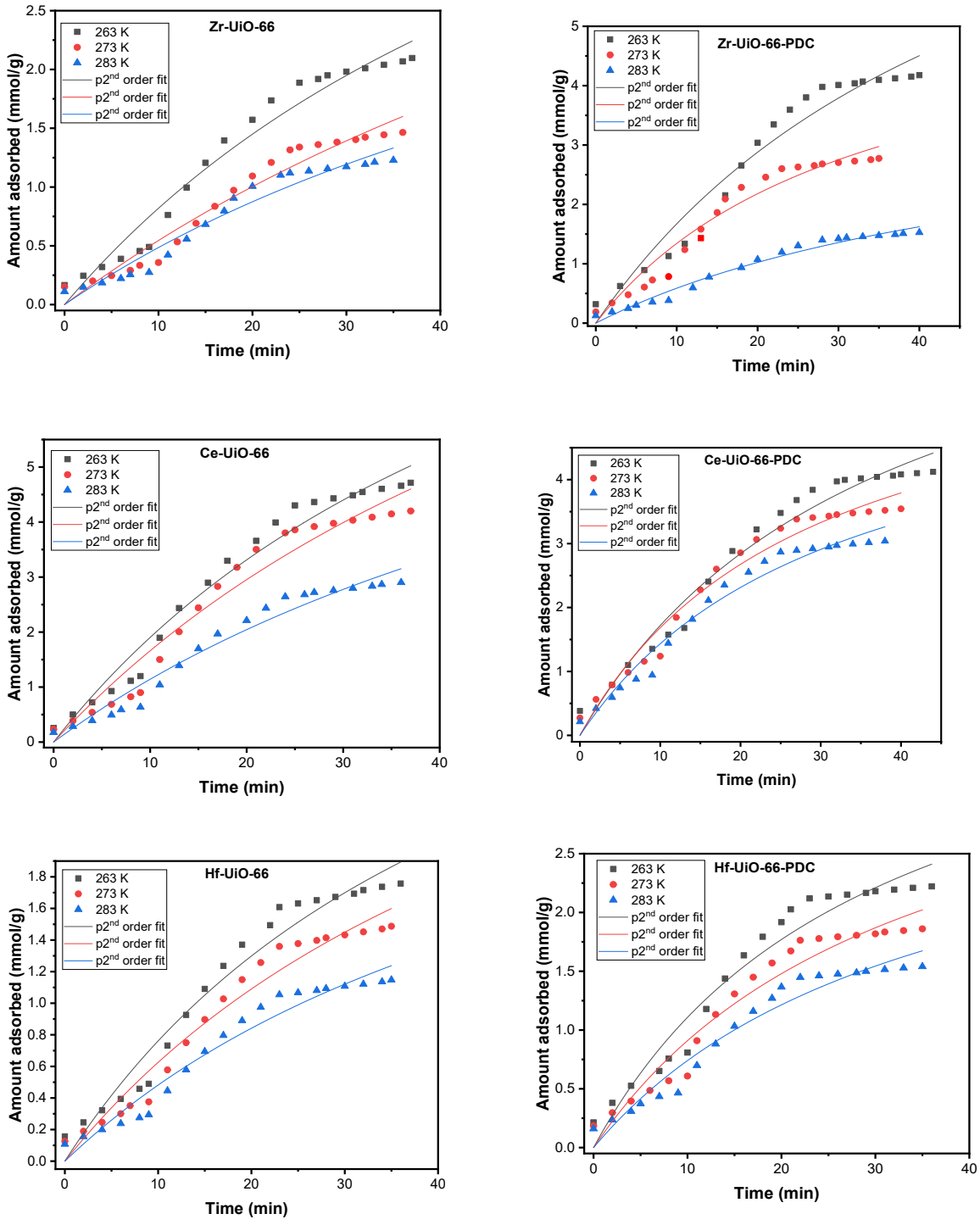

Figure S16. Non-linear fit of pseudo-second order kinetic model.

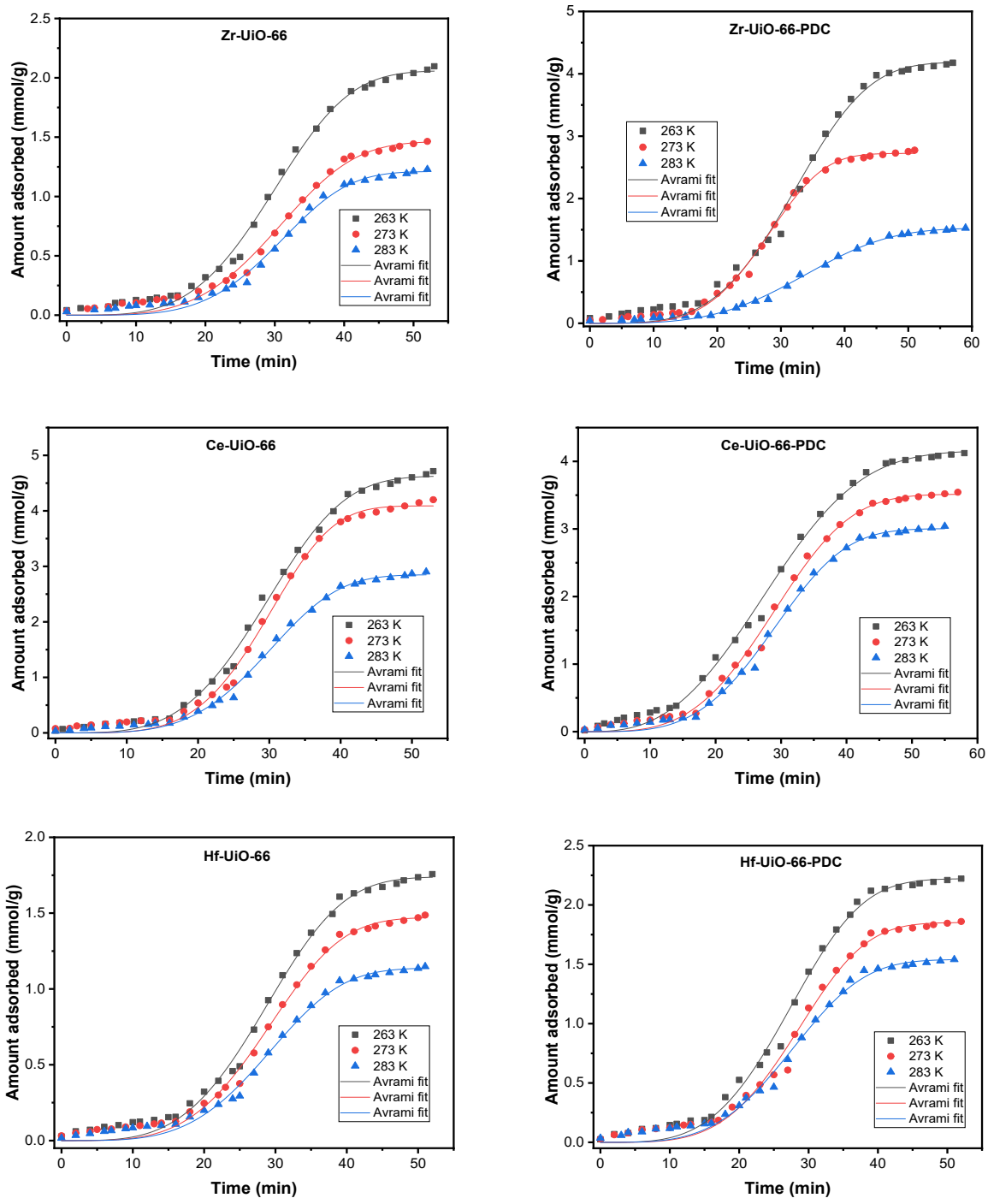

Figure S17. Effect of temperature on curves of CO_2 adsorption against time onto M-UiO-66 (M = Zr (IV), Ce (IV), Hf (IV)) with BDC or PDC linker.

Rate-limiting kinetic model

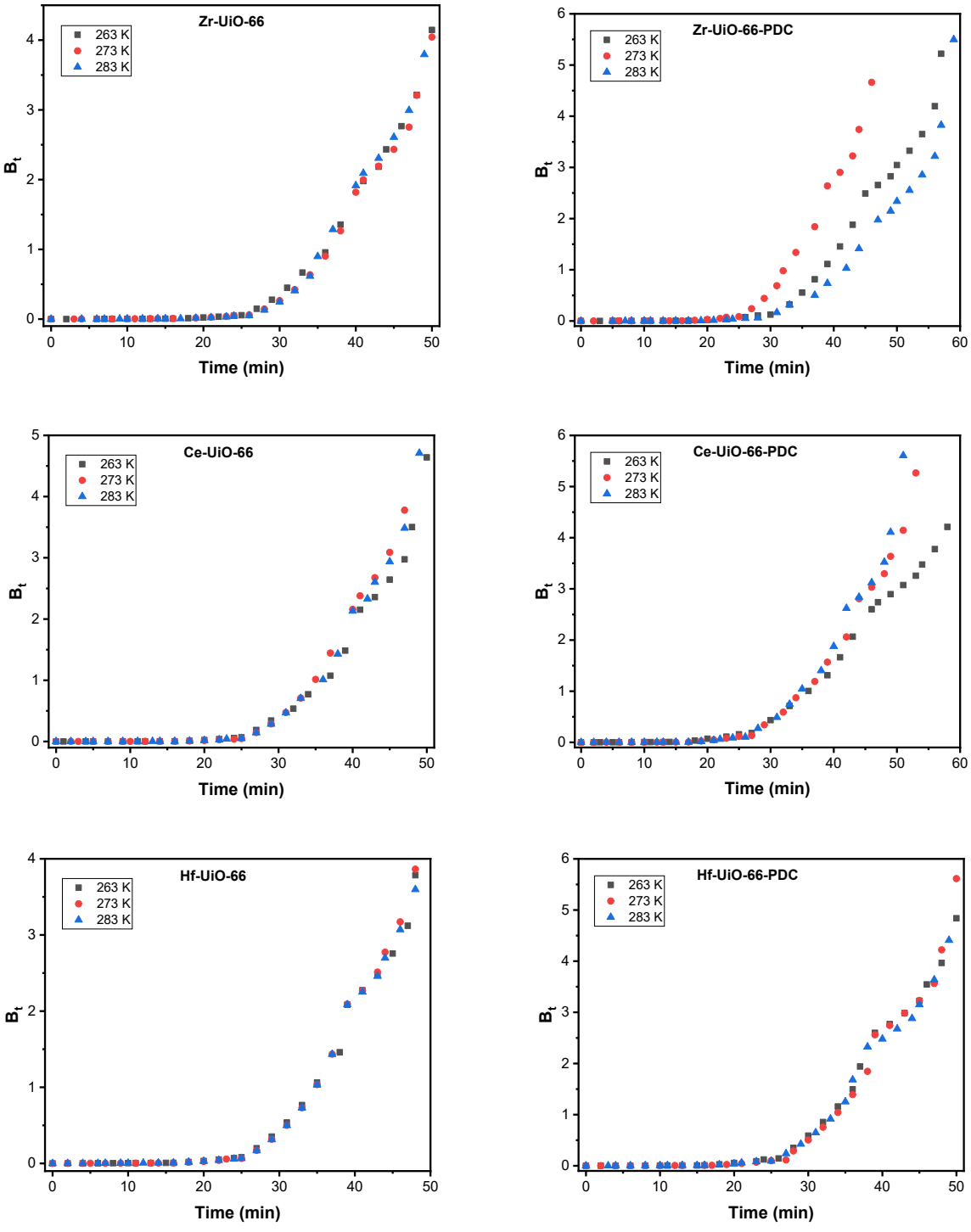

Figure S18. Plots of Boyd's film diffusion model for CO_2 adsorption onto M-UiO-66 with BDC or PDC linker under different temperatures.

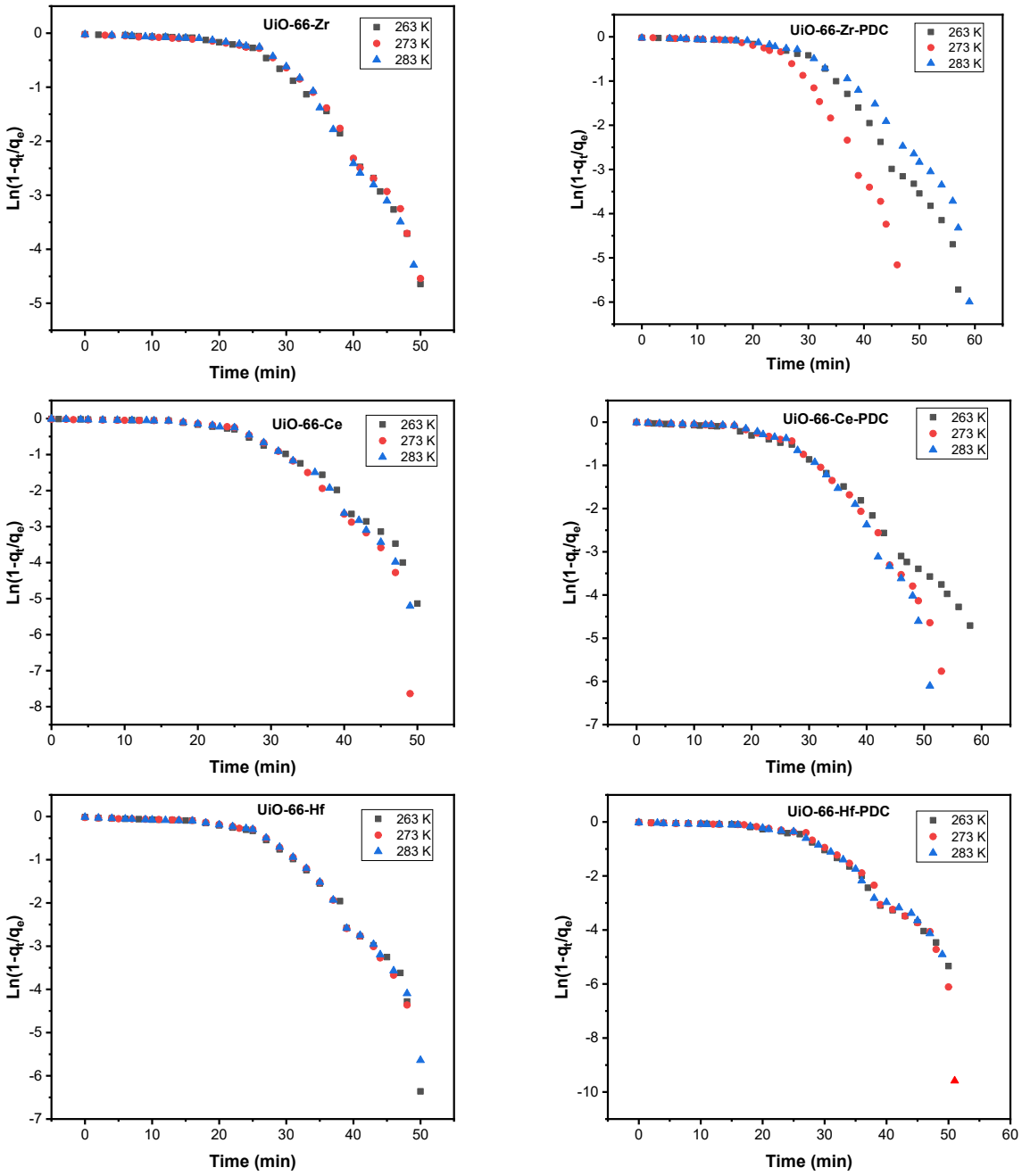

Figure S19. Plots of interparticle diffusion model for CO_2 adsorption onto M-UiO-66 with BDC or PDC linker under different temperatures.

Table S12. Linear fitting parameters of interparticle diffusion model.

Material	Temperature	Slope	Intercept	R^2
UiO-66-Zr	263 K	-0.08619	1.07412	0.81648
	273 K	-0.0973	1.09153	0.76701
	283 K	-0.07941	1.13155	0.79124
UiO-66-Zr-PDC	263 K	-0.08039	0.95016	0.79213
	273 K	-0.07721	0.89019	0.78001
	283 K	-0.0778	0.9457	0.77116
UiO-66-Ce	263 K	-0.08329	0.93442	0.77914
	273 K	-0.09798	1.14522	0.66041
	283 K	-0.08561	0.97891	0.75912
UiO-66-Ce-PDC	263 K	-0.08051	0.81262	0.89778
	273 K	-0.09418	1.10393	0.81448
	283 K	-0.09666	1.14354	0.78223
UiO-66-Hf	263 K	-0.09319	1.08837	0.75149
	273 K	-0.08061	0.87309	0.78521
	283 K	-0.08856	0.99759	0.77101
UiO-66-Hf-PDC	263 K	-0.09853	1.09127	0.8262
	273 K	-0.10121	1.18231	0.7802
	283 K	-0.09254	1.02646	0.81829

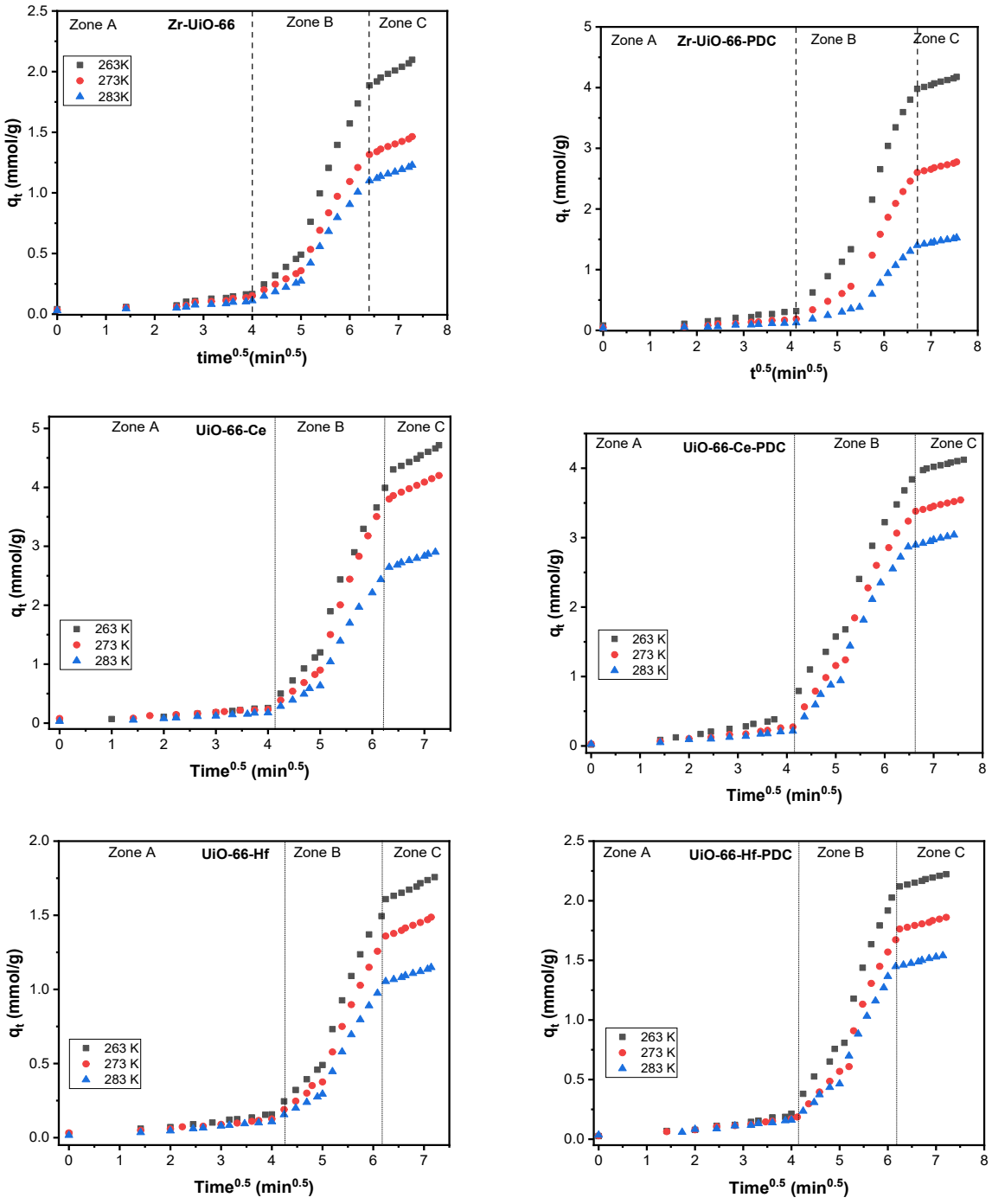

Figure S20. Plots of intraparticle diffusion model onto M-UiO-66 with BDC or PDC linker under different temperatures.

Isosteric Heat

Calculations of the isosteric heats using the Clausius-Clapeyron equation were performed with a temperature difference of 20 K.

Table S13. Short bibliographic research on CO_2 adsorption and reported isosteric heats of different MOFs.

Material	Adsorbate	Experimental conditions	Amount adsorbed (mmol g^{-1})	Q_{st} (kJ mol^{-1}) a = Zero/Low coverage b = High coverage	Ref.
Hf-UiO-66	CO_2	273-298 K and 1 bar	2,38	22,8[a]	11
Hf-UiO-66-NH_2	CO_2	273-298 K and 1 bar	3,99	25,6[a]	11
Hf-UiO-66-$(OH)_2$	CO_2	273-298 K and 1 bar	4,93	28,4[a]	11
Hf-UiO-66-$(COOH)_2$	CO_2	273-298 K and 1 bar	1,67	28,2[a]	11
Hf-UiO-66-F_4	CO_2	273-298 K and 1 bar	1,23	23,4[a]	11
Zr-UiO-67-BBS	CO_2	273-298 K and 760 torr	4,84	26,5[a]; 22,9[b]	12
Hf-UiO-67-BBS	CO_2	273-298 K and 760 torr	4,45	25,1[a]	12
Zr-UiO-67	CO_2	273-298 K and 760 torr	2,17	18,5[a]	12
Zr-UiO-66-$(OH)_2$-50	CO_2	25-35˚C and 100 kPa	4,83	39,6[a]	13
Zr-UiO-66-$(OH)_2$-250	CO_2	25-35˚C and 100 kPa	5,63	31,5[a]	13
Mg-MOF-74	CO_2	273-296 K and 1 bar	8	47[a]; 30[b]	14
Co-MOF-74	CO_2	273-296 K and 1 bar	7,1	37[a]; 36[b]	14
Ni-MOF-74	CO_2	273-296 K and 1 bar	5,8	41[a]; 34[b]	14
Carbonized MOF-5	CO_2	40-100 ˚C and 40 bar	2,43 (1 bar)	18[a]; 12,5[b]	15
Zr-UiO-66-1HCl	CO_2	298-318 K and 1 bar	1,66	25,9[a]	16
Zr-UiO-66-2FA	CO_2	298-318 K and 1 bar	1,42	21,5[a]	16
Zr-UiO-66	CO_2	263-283 K and 95 kPa	2,10	29,5[a]; 26,2[b]	This work
Zr-UiO-66-PDC	CO_2	263-283 K and 95 kPa	4,17	45,5[a]; 66,0[b]	This work
Hf-UiO-66	CO_2	263-283 K and 95 kPa	1,76	31,8[a]; 23,7[b]	This work
Hf-UiO-66-PDC	CO_2	263-283 K and 95 kPa	2,22	3,65[a]; 29,6[b]	This work
Ce-UiO-66	CO_2	263-283 K and 95 kPa	4,71	24,9[a]; 26,2[b]	This work
Ce-UiO-66-PDC	CO_2	263-283 K and 95 kPa	4,12	21,5[a]; 30,5[b]	This work

The tabulated amount adsorbed corresponds to the captured adsorbent at the maximum pressure and the minimal temperature.

Q_{st} calculated for each temperature combination.
Note that the average Q_{st} curve is hided by the 263-283 K Q_{st} curve.

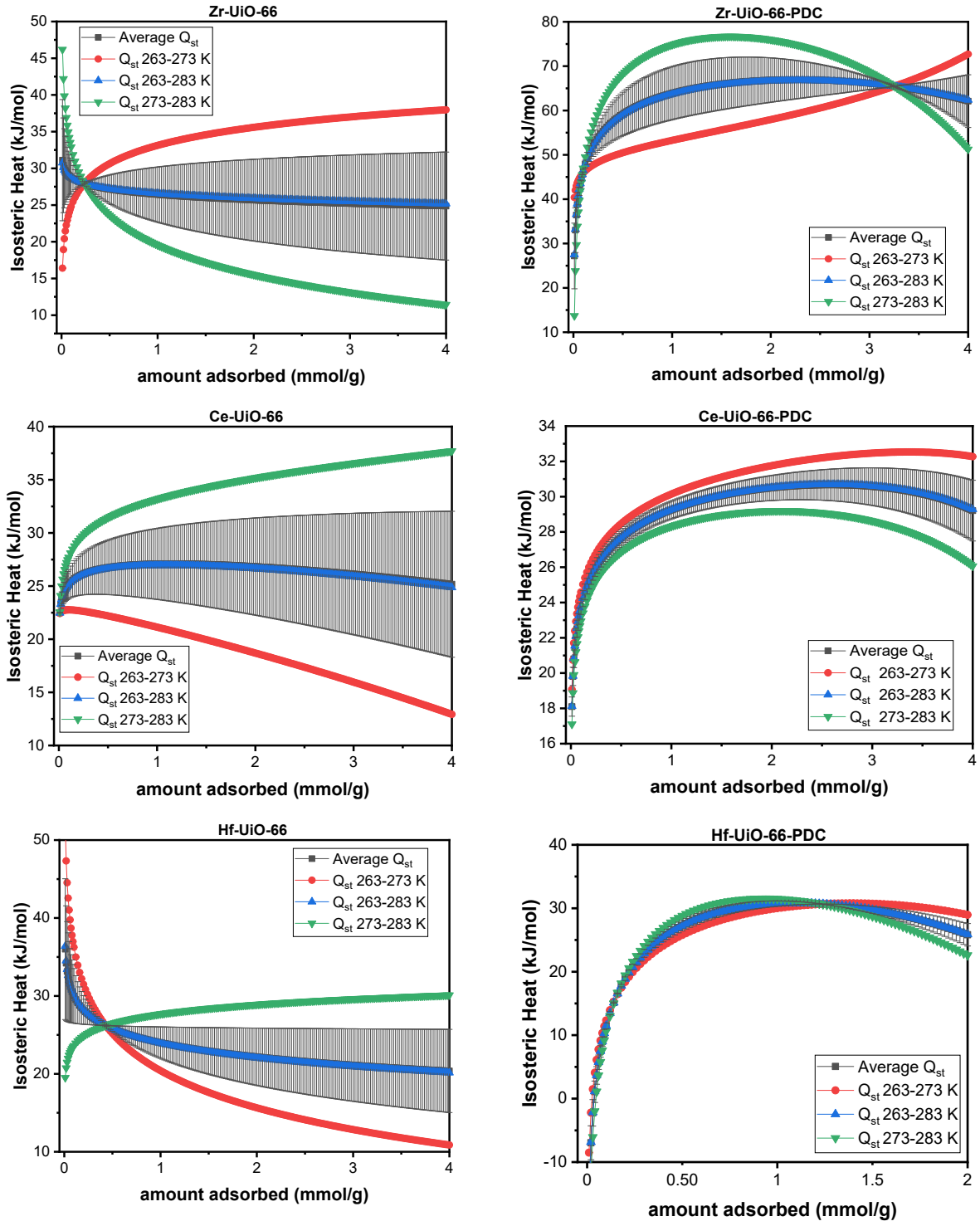

Figure S21. Q_{st} calculated for all temperature combinations.

Different perspectives of the isosteric heats.

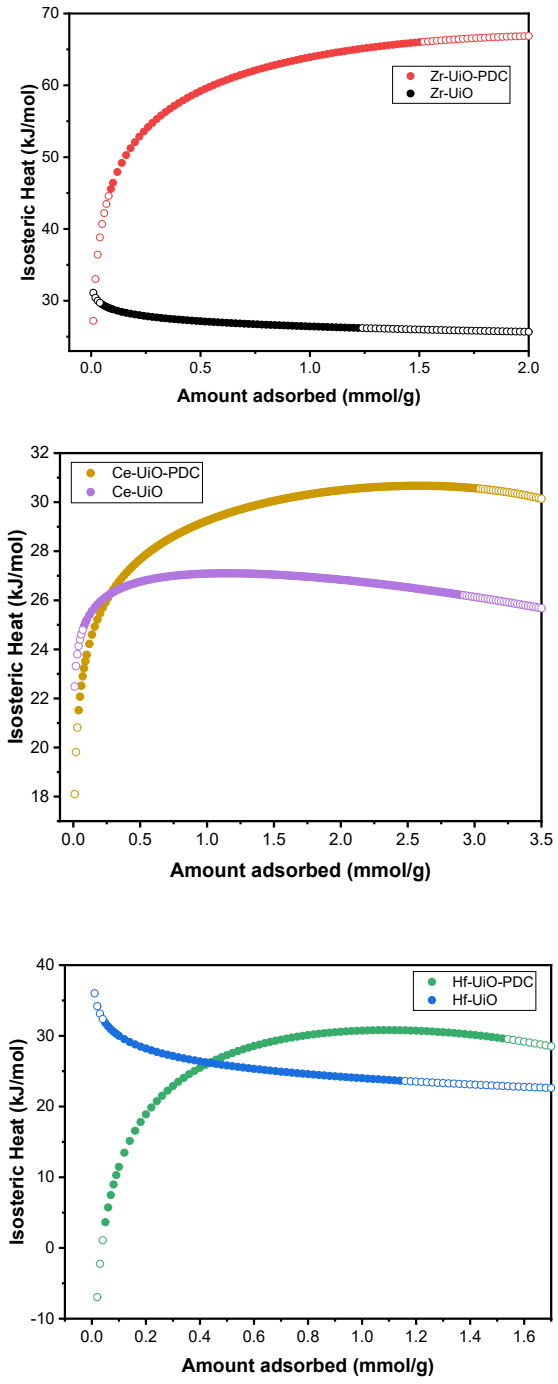

Figure S22. Isosteric heat in function of the amount adsorbed organized by metal center.

References

1 M. J. Katz, Z. J. Brown, Y. J. Colón, P. W. Siu, K. A. Scheidt, R. Q. Snurr, J. T. Hupp and O. K. Farha, *Chemical Communications*, 2013, **49**, 9449–9451.

2 M. Lammert, M. T. Wharmby, S. Smolders, B. Bueken, A. Lieb, K. A. Lomachenko, D. De Vos and N. Stock, *Chemical Communications*, 2015, **51**, 12578–12581.

3 S. Waitschat, D. Fröhlich, H. Reinsch, H. Terraschke, K. A. Lomachenko, C. Lamberti, H. Kummer, T. Helling, M. Baumgartner, S. Henninger and N. Stock, *Dalton Transactions*, 2018, **47**, 1062–1070.

4 G. C. Shearer, S. Chavan, J. Ethiraj, J. G. Vitillo, S. Svelle, U. Olsbye, C. Lamberti, S. Bordiga and K. P. Lillerud, *Chemistry of Materials*, 2014, **26**, 4068–4071.

5 M. J. Cliffe, W. Wan, X. Zou, P. A. Chater, A. K. Kleppe, M. G. Tucker, H. Wilhelm, N. P. Funnell, F. X. Coudert and A. L. Goodwin, *Nat Commun*, , DOI:10.1038/ncomms5176.

6 R. C. Klet, Y. Liu, T. C. Wang, J. T. Hupp and O. K. Farha, *J Mater Chem A Mater*, 2016, **4**, 1479–1485.

7 I. A. Lázaro, *Eur J Inorg Chem*, 2020, **2020**, 4284–4294.

8 S. Huang, D. G. Truhlar, A. Tang, X. He, H. Yin, Y. Li and Y. Zhang, *Journal of Physical Chemistry C*, 2021, **125**, 9679–9687.

9 C. Pazo-Carballo, E. Blanco, E. Camu, A. Leiva, Y. Hidalgo-Rosa, X. Zarate, A. B. Dongil, E. Schott and N. Escalona, *ACS Appl Nano Mater*, , DOI:10.1021/acsanm.2c05555.

10 Y. Wei, A. Tang, X. He, H. Chen, H. Yin, Y. Li, Y. Zhang and S. Huang, *Journal of Physical Chemistry C*, 2022, **126**, 4286–4295.

11 Z. Hu, A. Nalaparaju, Y. Peng, J. Jiang and D. Zhao, *Inorg Chem*, 2016, **55**, 1134–1141.

12 P. Xydias, I. Spanopoulos, E. Klontzas, G. E. Froudakis and P. N. Trikalitis, *Inorg Chem*, 2014, **53**, 679–681.

13 T. K. Vo, V. C. Nguyen, D. T. Quang, B. J. Park and J. Kim, *Microporous and Mesoporous Materials*, , DOI:10.1016/j.micromeso.2020.110746.

14 S. R. Caskey, A. G. Wong-Foy and A. J. Matzger, *J Am Chem Soc*, 2008, **130**, 10870–10871.

15 W. Kukulka, K. Cendrowski, B. Michalkiewicz and E. Mijowska, *RSC Adv*, 2019, **9**, 18527–18537.

16 W. Liang, C. J. Coghlan, F. Ragon, M. Rubio-Martinez, D. M. D'Alessandro and R. Babarao, *Dalton Transactions*, 2016, **45**, 4496–4500.